analytical chemistry

pubs.acs.org/ac

Article

Characterization of Unbranched Ubiquitin Tetramers by Combining Ultraviolet Photodissociation with Proton Transfer Charge Reduction Reactions

Aarti Bashyal, Sean D. Dunham, and Jennifer S. Brodbelt*

Cite This: *Anal. Chem.* 2023, 95, 14001−14008

Read Online

ACCESS | Metrics & More | Article Recommendations | Supporting Information

ABSTRACT: Polyubiquitination is an important post-translational modification (PTM) that regulates various biological functions. The linkage sites and topologies of polyubiquitination chains are important factors in determining the fate of polyubiquitinated proteins. Characterization of polyubiquitin chains is the first step in understanding the biological functions of protein ubiquitination, but it is challenging owing to the repeating nature of the ubiquitin chains and the difficulty in deciphering linkage positions. Here, we combine ultraviolet photodissociation (UVPD) mass spectrometry and gas-phase proton transfer charge reduction (PTCR) to facilitate the assignment of product ions generated from Lys6-, Lys11-, Lys29-, Lys33-, Lys48-, and Lys63-linked ubiquitin tetramers. UVPD results in extensive fragmentation of intact proteins in a manner that allows the localization of PTMs. However, UVPD mass spectra of large proteins (>30 kDa) are often congested due to the overlapping isotopic distribution of highly charged fragment ions. UVPD + PTCR improved the identification of PTM-containing fragment ions, allowing the localization of linkage sites in all six tetramers analyzed. UVPD + PTCR also increased the sequence coverage obtained from the PTM-containing fragment ions in each of the four chains of each tetramer by 7 to 44% when compared to UVPD alone.

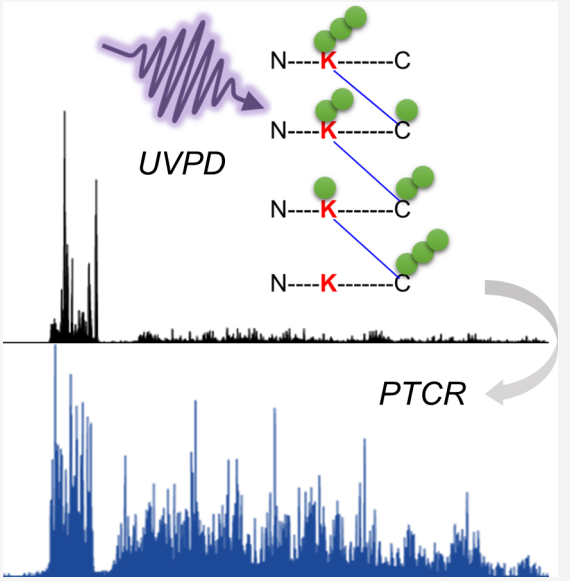

INTRODUCTION

Ubiquitin (Ub), a 76 amino-acid polypeptide, can form an isopeptide bond with either a substrate protein or another Ub.[1] Ubiquitin ligases aid in the formation of isopeptide bonds between the C-terminal glycine of Ub and the lysine residue of another Ub or a substrate protein in the process called ubiquitination.[1] Alternatively, deubiquitinases (DUBs) promote the hydrolysis of isopeptide bonds to liberate free Ub during the process of deubiquitination.[2] The equilibrium between ubiquitination and deubiquitination is crucial to maintaining normal cellular functions and homeostasis.[2] Ubiquitination is an important post-translational modification (PTM) involved in several physiological activities, including proteasomal degradation, cell cycle regulation, intracellular transport, kinase recognition, immunological response, and DNA damage repair, among others.[3−5] Dysfunction of the ubiquitin signaling pathway leads to cancer and metabolic, neurological, and immunological diseases.[2,6−10] The N-terminus (M1) and seven lysines (K6, K11, K27, K29, K33, K48, and K63) of a Ub molecule can attach to the C-terminal glycine of another Ub molecule to form polymers (polyUb) of different lengths, affording significant diversity in the resulting structures and functions.[11] The heterogeneity of ubiquitination is further amplified because several Ub molecules can be linked together at the same or different lysines to form chains of different lengths, linkages, and architectures.[11] Depending on the structural, spatial, and architectural diversity, protein ubiquitination imparts distinct biological functions.[12,13] For example, Lys48-linked ubiquitination is associated with proteasomal degradation, Lys27-linked polyubiquitination is associated with DNA damage repair, and Lys63-linked polyubiquitination plays a role in cellular signaling.[14] It is challenging to characterize protein ubiquitination due to its large size, low abundance, heterogeneity, and dynamic regulation in biological systems. Despite the challenges, comprehensive characterization of Ub chains is essential to

Received: June 15, 2023
Accepted: August 22, 2023
Published: September 7, 2023

Downloaded via UNIV OF TEXAS AT AUSTIN on April 2, 2024 at 17:55:44 (UTC).
See https://pubs.acs.org/sharingguidelines for options on how to legitimately share published articles.

ACS Publications

© 2023 American Chemical Society

https://doi.org/10.1021/acs.analchem.3c02618
Anal. Chem. 2023, 95, 14001−14008

understand how the diversity of this PTM influences various biological processes.[11]

Tandem mass spectrometry (MS/MS) is a technique of choice for characterizing and localizing various PTMs, including ubiquitination.[15] Bottom-up MS/MS is the gold standard in proteomics to understand ubiquitin biology in a high-throughput manner.[16−20] In the bottom-up approach, trypsin cleaves after the C-terminal Arg (R74), leaving behind a diglycine tag (GG) as a much smaller surrogate marker at the ubiquitination site of a modified protein. This bottom-up strategy facilitates high-throughput analysis of polyUb chains and polyubiquitinated proteins; however, the truncation of polyUb during trypsin digestion prohibits the discernment of the chain length or connectivity (linkage pattern).[13] The alternative middle-down approach utilizes limited proteolysis (i.e., native trypsinization) to cleave Ub chains selectively at R74, producing diglycine-tagged Ub monomers that are an optimal size for MS/MS analysis.[21−24] An engineered viral protease (leader protease, Lbpro) also specifically cleaves at R74, generating diglycine-modified Ub monomers for middle-down analysis.[25] Despite losing linkage-type information at the branching points, the middle-down approach is a compelling strategy because it retains linkage and branching information while generating Ub monomers that can be easily analyzed using MS/MS to localize the linkage sites in the original proteins.[26] Furthermore, it allows relative quantitation of the digestion products to determine chain stoichiometry and the extent of branching.[24] Another method, Ub chain restriction (UbiCRest), hydrolyzes the Ub polymers or polyubiquitinated proteins using complementary linkage-specific DUBs in parallel. The hydrolysis products are then detected using a gel-based assay to elucidate linkage types and architecture of heterotypic chains.[27] However, the cross-specificity of some DUBs warrants the necessity for LC-MS/MS analysis to validate the gel-based results.[26]

Top-down mass spectrometry coupled with advanced ion activation methods for MS/MS retains the structural information embedded in the polyUb chains and can reveal the linkage position, branching patterns, and chain length without additional treatments.[26] Ion activation methods like electron transfer dissociation supplemented with higher energy collision dissociation (known as EThcD)[28,29] and ultraviolet photodissociation (UVPD)[30] facilitate the analysis of larger molecules by producing rich fragmentation patterns.[31] UVPD has been used to characterize combinatorial patterns of modifications and has shown promising results for the analysis of intact proteins.[30−33] UVPD and electron-based methods have been used to elucidate the linkage patterns of intact ubiquitin polymers.[28−30,34] ETD was used to reveal the linkage and branching patterns of intact Ub-trimers.[28] Electron transfer dissociation supplemented with collisional activation (known as ETciD) was used to elucidate the structure of Ub-tetramers,[34] and EThcD was used to access the linkage sites in two-component branched proteins.[29] 193 nm UVPD was used to characterize Lys48- and Lys63-linked ubiquitin polymers based on the increased ion current of a series of N-terminal fragment ions devoid of modifications generated from each monomer up to the linkage site.[30] However, this method was not feasible for Lys6- or Lys11-linked chains because the key diagnostic fragment ions exhibited low S/N noise and other artifacts during deconvolution.[30]

UVPD generates a diverse array of fragment ion types (a, $a+1$, b, c, x, $x+1$, y, $y-1$, and z), facilitating extensive sequence coverage and PTM localization in proteins.[30,32,35,36] However, the increased array of highly charged fragment ions from large proteins impedes their analysis due to overlapping isotopic distributions and reduced signal-to-noise (S/N) ratios.[37−41] To alleviate this issue, gas-phase proton transfer charge reduction (PTCR) have been performed on UVPD product ions.[33,37] Reacting large highly charged UVPD product ions with reagent anions produces charge-reduced fragment ions and disperses them across a larger m/z domain, thus decreasing the overlap in the isotopic distributions.[33,37] This process also increases the S/N ratios of large PTM-localizing fragment ions, thus improving their deconvolution and identification, hence increasing the sequence coverage of larger proteins.[33,37] Here, we capitalize on the attributes of UVPD to generate informative PTM-localizing fragment ions and PTCR to decongest the MS/MS spectra to aid in the characterization of six unbranched ubiquitin tetramers linked at Lys6, Lys11, Lys29, Lys33, Lys48, and Lys63, respectively. We specifically aim to increase the identification of PTM-containing fragment ions larger than the size of a Ub monomer (8.6 kDa) and up to the size of a Ub tetramer (34 kDa).

EXPERIMENTAL SECTION

Ubiquitin tetramers linked at K6, K11, K29, K33, K48, and K63 were purchased from Boston Biochem, Inc., Cambridge, MA. Proteins were diluted to ∼6 μM in a 50:50 solution of acetonitrile:water with 0.5% formic acid. Experiments were performed on a modified Thermo Fisher Scientific Orbitrap Fusion Lumos mass spectrometer, enabling 193 nm UVPD in the dual-pressure linear ion trap (LIT) using an excimer laser.[42] Protein solutions were infused using a static tip applying a voltage of 1−1.1 kV. Intact protein mode (ion routing multipole pressure of 0.002 Torr), high mass range (m/z 400−3000), and a resolving power of 240,000 at m/z 200 were used for data acquisition. The precursor ion (z = 25+) was isolated using an isolation width (IW) of 2 m/z, transferred to the high-pressure LIT cell, and activated using a single laser pulse of 0.8 mJ. For UVPD + PTCR experiments, UVPD product ions were reisolated in 10 "windows" using an IW of 60 m/z (with 10 m/z overlap) to cover the congested regions of the MS^2 spectra (1200 to 1600 m/z). This includes five "windows" below the precursor and five "windows" above the precursor, excluding the precursor (z = 25+) at 1369.2 m/z. The product ions were reacted with the PTCR reagent (nitrogen adduct of fluoranthene, m/z 216) for 10 ms, and the resulting charge-reduced product ions were mass analyzed in the Orbitrap.[37] UVPD experiments used 400 transient averages, and UVPD + PTCR experiments used 150 transients per isolation window. Precursor ion automatic gain control (AGC) was set to 1E6 charges, and that for reagent ions was set to 2E5 charges.

MS^2 and MS^3 spectra were collected in triplicate and deconvoluted by using the Xtract algorithm with an S/N of three. Fragment maps were visualized using ProSight Lite (http://prosightlite.northwestern.edu/) using a mass tolerance of 10 ppm. Fragment ions identified in only one of three replicates were discarded. The data and the list of matched fragment ions are available in the jPOST repository under accession numbers PXD043027 (ProteomeXchange) and JPST002201 (jPOST). Data can be previewed using the access key 5462 at https://repository.jpostdb.org/preview/1708631411648b46058e52a.

https://doi.org/10.1021/acs.analchem.3c02618
Anal. Chem. 2023, 95, 14001−14008

RESULTS AND DISCUSSION

In this study, we characterize six unbranched ubiquitin tetramers using UVPD and UVPD + PTCR. The sequence, linkage patterns, and nomenclature of all six tetramers, including Ub-^{6}Ub-^{6}Ub-^{6}Ub, Ub-^{11}Ub-^{11}Ub-^{11}Ub, Ub-^{29}Ub-^{29}Ub-^{29}Ub, Ub-^{33}Ub-^{33}Ub-^{33}Ub, Ub-^{48}Ub-^{48}Ub-^{48}Ub, and Ub-^{63}Ub-^{63}Ub-^{63}Ub (K6-, K11-, K29-, K33-, K48-, and K63-linked tetramers, respectively), are illustrated in Scheme S1.[34] The ESI mass spectra of the six isomeric tetramers exhibit broad charge state distributions typical of denatured proteins and yield the same monoisotopic mass (Figure S1).

For initial MS/MS characterization, three different charge states (z = 25+, 29+, and 33+) of the K11-linked tetramer were compared using one laser pulse at 0.8 mJ for UVPD and 60 m/z windows for UVPD + PTCR. Examples of UVPD mass spectra and deconvoluted UVPD mass spectra are shown in Figures S2 and S3, respectively. Extensive fragmentation of Ub tetramers was observed, and the dense spectra contained numerous low-abundance but highly informative fragment ions. Previously, K48- and K63-linked tetramers were identified by monitoring the abundance of PTM-devoid a-ion series (a_{47} to a_{62}) originating from the ubiquitin monomers.[30] For the present study, the abundances of PTM-devoid a + 1 ions originating directly before and at the linkage site for the six tetramers are depicted in Figures S4 and S5. Notably, PTM-devoid fragment ions exhibit low abundances or are absent for K6- and K11-linked tetramers, preventing their use for identification or relative quantitation.[30] Therefore, we employ PTM-containing fragment ions to differentiate these isomers. The 25+ charge state resulted in the identification of the highest number of PTM-containing fragment ions for both UVPD and UVPD + PTCR (Figure S6) and was chosen for the subsequent study. The 25+ charge state of the K11-linked Ub tetramer was also used for UVPD optimization by subjecting it to a single laser pulse of variable energy (0.5, 0.8, 1.0, and 1.5 mJ). A pulse energy of 0.8 mJ was found to be the most effective, producing informative fragment ions without PTM loss, and was used for subsequent experiments.

For the representative UVPD mass spectra in Figure S2, the particularly dense sections below and above the precursor are highlighted. These regions contain most of the larger, highly charged fragment ions for which the low abundances and overlapping isotopic distributions obscure facile assignment. Therefore, the deconvoluted MS/MS spectra exhibit fewer fragments in the higher m/z range and are denser in the region below 10 kDa (Figure S3). Few fragment ions in these regions of high spectral density are successfully harvested, thus emphasizing the potential dividends captured by coupling UVPD with PTCR to redistribute overlapping fragment ions over a broader m/z range and alleviate overlap of ions.

To capitalize on the benefits of PTCR, small sections (narrow m/z ranges) of ions from the m/z regions lower and higher than the precursor were isolated and reacted with the PTCR reagent anion to allow charge reduction, thus decreasing the charge states of the fragment ions and dispersing them over a greater m/z range. For this strategy, the surviving precursor ion was always excluded from the PTCR reactions to avoid the production of uninformative charge-reduced precursor ions. The performance of three different strategies for segmenting the fragment ion population based on different m/z windows (w30 (30 m/z window), w60 (60 m/z window), and w120 (120 m/z window)) was assessed for UVPD + PTCR using the K48-linked tetramer (z = 25+) (Table S1). The sequence coverage, number of matching fragments, and fragment mass distribution for each of the four chains of the K48-linked tetramer were evaluated for the identification of PTM-containing sequence ions that are larger than the mass of a Ub monomer. The deconvoluted mass lists from each window were combined and mapped onto the sequence of a Ub monomer representing the distal, *β-endo*, *α-endo*, and proximal chains, as defined in Figure 1.

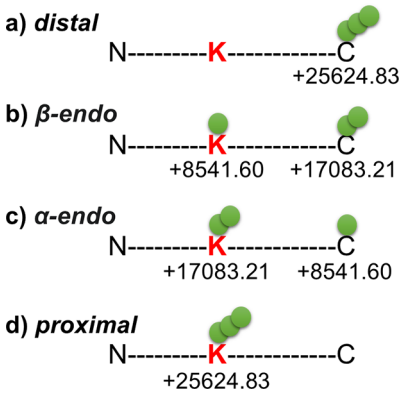

Figure 1. Depiction of the four chains of a Ub tetramer. Only the N-terminus, lysine, and C-terminus are shown. The highlighted Lys (K), involved in the linkage, may represent K6, K11, K27, K33, K48, or K63 for the respective tetramer. Each green circle represents a Ub monomer. (a) Distal Ub chain has three Ub attached to the C-terminus; (b) *β-endo* Ub chain has one Ub attached to Lys and two Ub attached to the C-terminus; (c) *α-endo* Ub chain has two Ub attached to Lys and one Ub attached to the C-terminus; and (d) proximal Ub chain has three Ub attached to the Lys and a free C-terminus. Each tetramer may be represented as any of the four different chains (a–d).

We evaluated three metrics: (i) the number of PTM-containing fragment ions, (ii) sequence coverage, and (iii) the mass distribution of fragment ions for the three different isolation widths (further discussed in Figure S7). The 30 m/z windows outperformed the 60 m/z windows for all four Ub chains of the K48-linked tetramer. However, the improved performance metrics when using the 30 m/z windows come at the cost of increased acquisition time, arising from the greater number of PTCR events used to probe the narrower and more numerous 30 m/z windows. Therefore, a PTCR window size of 60 m/z was used owing to the significantly shorter data acquisition time.

The PTM-devoid fragment ions are shared among all four ubiquitin chains in a tetramer and do not help assess the linkage site, whereas PTM-containing fragment ions allow the distinction of one tetramer from another. The PTM-containing ions generated upon UVPD are primarily >17 kDa and are in low abundance, features that contribute to the difficulty in uncovering and assigning them. Ten 60 m/z windows in the UVPD mass spectra of the six Ub tetramers are shaded to show the most congested m/z regions lower and higher than the precursor (Figure S8), regions that are well-suited for PTCR. These sections of fragment ions (each with 10 m/z overlap between adjacent segments) were sequentially isolated and reacted with the PTCR anions for 10 ms. Representative UVPD + PTCR spectra for the K48-linked tetramer are shown in Figure S9, and the analogous deconvoluted mass spectra are

https://doi.org/10.1021/acs.analchem.3c02618
Anal. Chem. 2023, 95, 14001−14008

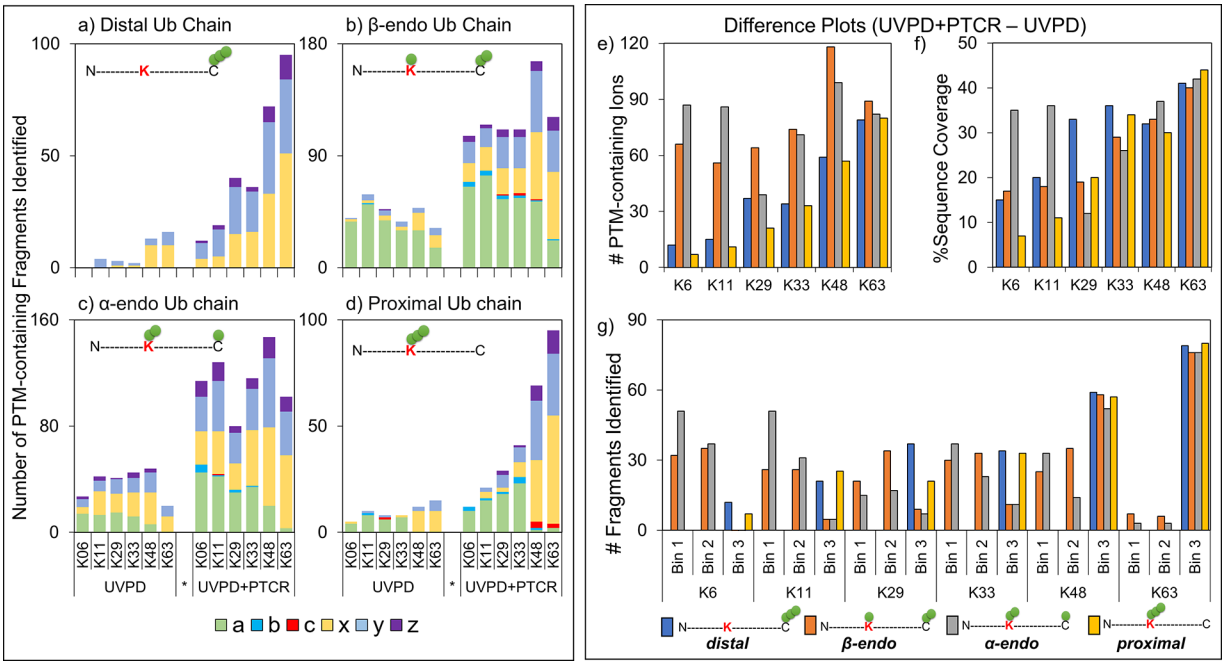

Figure 2. PTM-containing fragment ions are represented as the number of *a*, *b*, *c*, *x*, *y*, and *z* type ions for the (a) distal, (b) *β-endo*, (c) *α-endo*, and (d) proximal chains of the six tetramers (z = 25+) for UVPD and UVPD + PTCR (left panel). The difference (UVPD + PTCR − UVPD) in (e) the number of PTM-containing fragments identified, (f) sequence coverage obtained using PTM-containing fragments, and (g) the number of PTM-containing fragment ions across three mass bins for the six tetramers (z = 25+). The four colors represent the four Ub chains of the tetramer (right panel).

shown in Figure S10. The resulting product ions are dispersed in a wider m/z domain for all 10 windows. The deconvoluted UVPD + PTCR spectra reveal that the m/z regions higher than the precursor are populated with fragment ions >20 kDa, while the regions lower than the precursor encompass smaller fragment ions. The isotopic distributions of several fragment ions identified by UVPD + PTCR are shown in Figure S11 to illustrate the fits to theoretical isotopic patterns based on the molecular compositions of each ion.

Using the same 60 m/z window strategy, we systematically collected UVPD + PTCR spectra for all six tetramers (z = 25+). A single combined mass list was created from 10 deconvoluted spectra for each tetramer. Each mass list was matched against the sequence of a Ub monomer by creating templates that represent the four Ub chains (distal, *β-endo*, *α-endo*, and proximal), as depicted in Figure 1. The redundant PTM-devoid fragment ions were excluded from further analysis to focus on discovering specific trends exhibited by the informative PTM-containing fragment ions. To assess how the distribution of PTM-containing UVPD product ions (N-terminal *a*, *b*, *c*, and C-terminal *x*, *y*, and *z*) changed upon PTCR, we summarized the number of fragments identified for UVPD alone and UVPD + PTCR for each of the four chains (distal, *β-endo*, *α-endo*, proximal) of the six tetramers (Figure 2a−d). In addition, the relative portion of each type of fragment ion (N-terminal *a*, *b*, *c*, and C-terminal *x*, *y*, and *z*) is shown in Figure S12 for each of the four chains (distal, *β-endo*, *α-endo*, proximal). For each tetramer analyzed, the identification of C-terminal fragment ions (*x*,*y*,*z*) increased significantly for UVPD + PTCR, while the gain in the number of N-terminal ions upon UVPD + PTCR was less significant (Figure 2b−d). The biggest gains in the number of identified PTM-containing fragments upon PTCR occurred for the K48- and K63-linked tetramers, primarily due to the notable contribution of *x*, *y*, and *z*-type fragment ions which are more readily identified upon UVPD + PTCR. Moreover, the majority of the PTM-containing C-terminal fragment ions that contain K48 (xyz_{29} to xyz_{75}) or K63 (xyz_{14} to xyz_{75}) from the K48- and K63-linked tetramers have the same mass for each of the four Ub-chains and are more numerous than the number of possible PTM-containing C-terminal fragment ions generated from the K6, K11, K29, or K33 tetramers, causing more spectra congestion. Additionally, the sizes of C-terminal ions for K48- and K63-linked tetramers are smaller than those for K6- or K11-linked tetramers and are less prone to overlap (Table S2).

The number of PTM-containing fragment ions, sequence coverages derived from the PTM-containing fragments, and the number of identified fragments categorized in three different mass bins were evaluated for UVPD and UVPD + PTCR (Figure 2e−g). UVPD + PTCR resulted in the identification of more PTM-containing fragments, particularly those attributed to the *α-endo* and *β-endo* chains, thus increasing the sequence coverage for all four chains of the six tetramers (Figure 2e,f). With respect to the sizes of fragment ions and their impact on characterization of the tetramers, the first mass bin (8.6−17.1 kDa) encompasses the N-terminal fragments from the *β-endo* chain and the C-terminal fragments from the *α-endo* chain, and the second mass bin (17.1 to 25.6 kDa) encompasses the N-terminal fragments from the *α-endo* chain and C-terminal fragments from the *β-endo* chain (Table S2). The PTM-containing fragment ions from the proximal and distal chains for all six tetramers are >25 6 kDa and are grouped in the third mass bin. PTCR significantly improved the detection of fragment ions in the first mass bin from the *α-endo* and *β-endo* chains of the K6-, K11-, and K33-linked tetramers and in the third mass bin for K48- and K63-linked tetramers (Figure 2g). The total possible number of PTM-containing N-terminal fragment ions from the

https://doi.org/10.1021/acs.analchem.3c02618
Anal. Chem. 2023, 95, 14001−14008

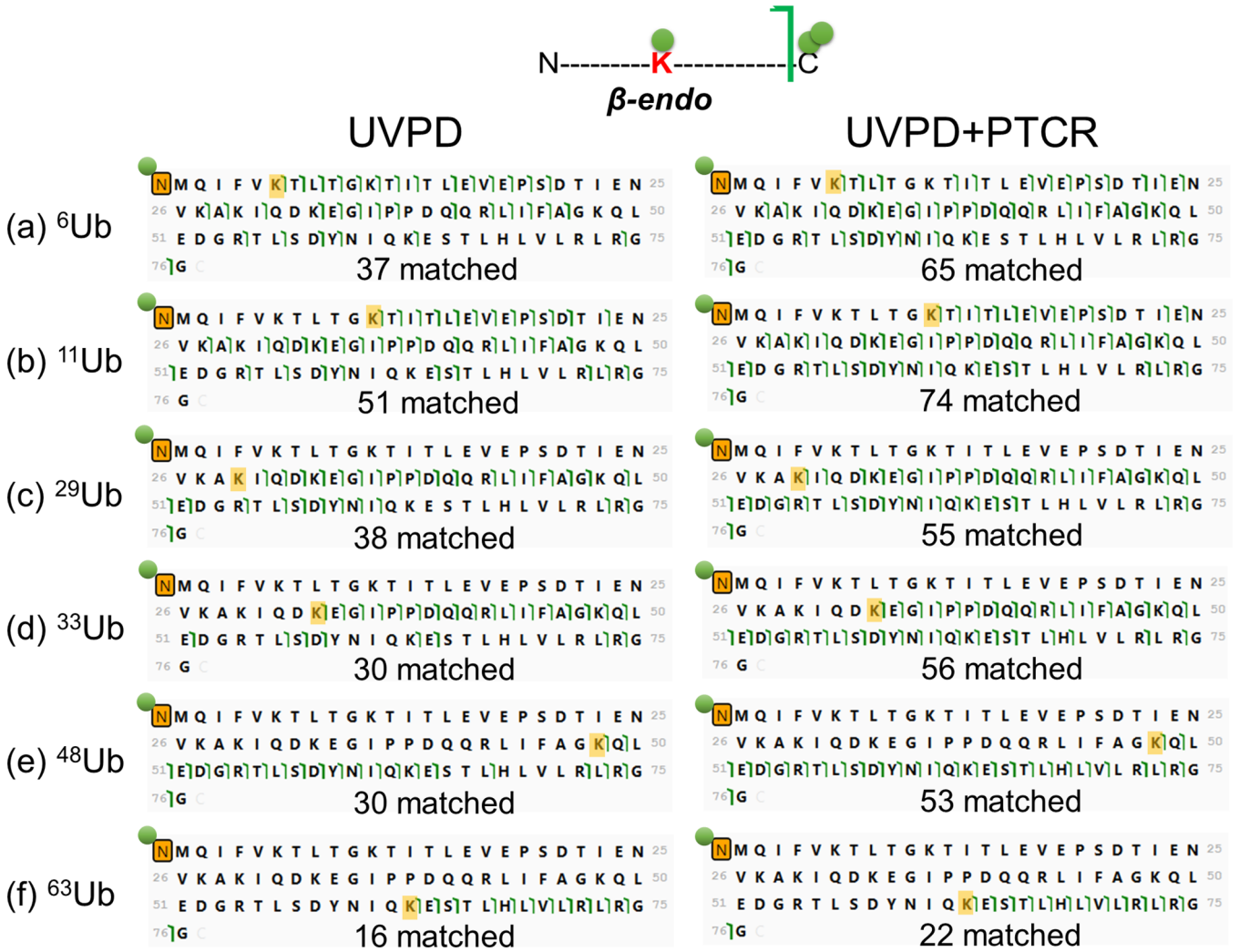

Figure 3. PTM-containing $a/a + 1$ identified from the *β-endo* chain using UVPD (left) and UVPD + PTCR (right) for the (a) K6-, (b) K11-, (c) K29-, (d) K33-, (e) K48-, and (f) K63-linked tetramers ($z = 25^+$) mapped onto the sequence of a Ub monomer. Linked lysines are highlighted in gold. The first *a*-ion is generated at or after the modified residue despite adding one Ub molecule (green circle) to the N-terminus (+8541.61 Da, shaded in orange). The addition of two Ub to the C-terminus is not shown.

K48- and K63-linked tetramers are significantly lower than those from the K6-, K11-, K29-, and K33-linked tetramers and hence is less frequently detected. The identification of PTM-containing C-terminal fragments from the *α-endo* chains (also in the mass range 8.6−17.1 kDa) is also enhanced upon PTCR, an outcome readily seen in Figure 2c.

The PTM-containing N-terminal fragments from the *α-endo* chain and the C-terminal fragments from the *β-endo* chain fall in the second mass bin, 17.1−25.6 kDa (Figure 2g, Bin 2). There is a gradual decline in the identification of PTM-containing fragments in the mass bin of 17.1−25.6 kDa as the position of the Ub-linkage site moves from K6 to K11 and onward to K63 primarily because the fragment ions become >25.6 kDa. As evidenced by the increase in the number of PTCR-identified fragments as the Ub-linkage site moves from K6 to K63, reinforcing that fragment ions larger than 25.6 kDa, ones previously obscured by overlapping isotopic distribution in the UVPD spectra, are uncovered by PTCR (Figure 2g, Bin 3). This outcome is also shown by the increased identification of new fragment ions upon UVPD + PTCR, specifically C-terminal ions of the distal and proximal chains, as they are notably larger than those originating from the *β-endo* and *α-endo* chains (Figure 2a,g). Collectively, these results show that PTCR effectively improves the detection of large product ions generated by UVPD by dispersing the ions across a broader m/z landscape.

Since the N-terminal fragment ions generated from the fragmentation of proximal and *endo* chains are more specific for each of the tetramers analyzed and aid in the discernment of linkage site, we focused on the PTM-containing N-terminal fragment ions, particularly *a* and $a + 1$ ions, that are often generated upon UVPD. The number of PTM-containing N-terminal fragment ions resulting from the dissociation of Ub tetramers is expected to decrease as the modification shifts from K6 to K63 owing to the placement of the modification relative to the N-terminus (see Scheme S2). The opposite is expected for the C-terminal fragment ions originating from the proximal chains (potential production of more PTM-containing C-terminal fragment ions as the modification shifts from K63 to K6), as illustrated in Scheme S3. To emphasize the impact of the PTM-containing *a* and $a + 1$ ions produced from UVPD and UVPD + PTCR, a multistep strategy was used to characterize the ubiquitin tetramers comprehensively. First, the PTM-containing N-terminal fragments (*a* and $a + 1$

https://doi.org/10.1021/acs.analchem.3c02618
Anal. Chem. 2023, 95, 14001−14008

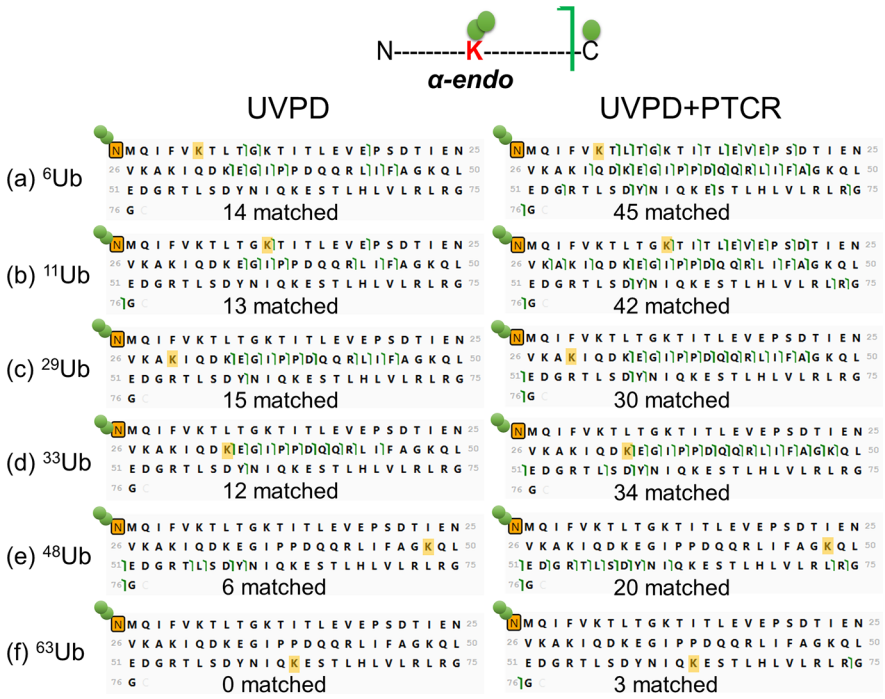

Figure 4. PTM-containing *a*/*a* + 1-type ions identified from the *α-endo* chain using UVPD (left) and UVPD + PTCR (right) for the (a) K6-, (b) K11-, (c) K29-, (d) K33, (e) K48-, and (f) K63-linked tetramers ($z = 25^+$) mapped onto the sequence of a Ub monomer. Linked lysines are highlighted in gold. Two Ub molecules (green circles) are added to the N-terminus (+17083.21 Da, shaded in orange). The addition of one Ub to the C-terminus is not shown.

ions) from the *β-endo* chains (with one Ub added to the N-terminus) of the six unbranched ubiquitin tetramers are mapped onto the sequence of a surrogate Ub monomer (Figure 3). This first step allows a more specific search and minimizes the identification of isobaric ions that may arise from other fragmentation channels. The PTM is placed on the N-terminus instead of the modified Lys to confirm that the smallest PTM-containing N-terminal product ions do not emerge until the true site of modification is reached for each of the six tetramers. For all six tetramers, UVPD + PTCR resulted in a greater number of identified product ions than UVPD alone but with fewer notable gains for the K63-linked tetramer. The lower gains for the K63-linked tetramer are attributed to the detection of fewer higher-mass fragment ions produced with low S/N; only a few sets of PTM-containing a_{63} to a_{76} ions are monitored for the K63-linked tetramer, thus limiting the potential gains from PTCR. Since the fragment ions generated from the *β-endo* chain are relatively small (e.g., a_6 ion of 9.3 kDa to a_{75} ion of 17 kDa), both UVPD and UVPD + PTCR identified sufficient fragment ions to allow the assignment of the site of modification readily.

Next sequence maps were created for the *α-endo* chains (with two Ub added to the N-terminus) for the six tetramers using UVPD and UVPD + PTCR (Figure 4). For these maps, the smallest PTM-containing *a*-ion (a_6) is 17.8 kDa, and the largest a_{75} ion is 25.6 kDa. UVPD + PTCR increased the identification of PTM-containing product ions for all six tetramers compared to UVPD alone, although only three new fragment ions were identified for the K63-linked tetramer upon PTCR. The PTM-containing N-terminal fragment ions from the proximal chain are all >26.3 kDa (Table S2), and very few are identified (Figure S13). Fewer than ten *a* and *a* + 1 ions were identified for each of the six tetramers using UVPD alone. Although UVPD + PTCR slightly increased the number of PTM-containing *a*-ions, very few backbone cleavages allowed for the confident assignment of the linkage sites. Additionally, the erroneous identification of the isobaric PTM-containing x_{37} + 1 ion (29904.1363 Da) as the a_{39} ion (29904.1324) for both the K48- and K63-linked tetramers (Figure S13e,f, right panel) hampered the linkage-site assignment.

As noted in Figure 2a–d, an increased number of informative PTM-containing C-terminal fragment ions were identified for the four chains upon UVPD + PTCR of all six tetramers, more specifically for the distal and proximal chains of the K48- and K63-linked tetramers. Therefore, to aid in the more comprehensive characterization of the six tetramers, complete sequence maps were created using PTM-containing fragment ions (all nine ion types generated upon UVPD *a*, *a* + 1, *x* + 1, *y* − 1, *x*, *z*, *b*, *c*, *y*). The sequence of a Ub monomer was used as a template to create four Ub-chains (distal, *β-endo*, *α-endo*, proximal) by adding the mass shifts at the modified Lys or the C-terminus. The four templates were combined to show the complete sequence maps for UVPD (left) and UVPD + PTCR (right) for K6-, K11-, and K29-linked tetramers (Figure S14) and for K33-, K48-, and K63-linked tetramers (Figure S15). UVPD + PTCR improved the identification of both N- and C-terminal PTM-containing fragment ions compared to UVPD alone, averaging the identification of over 35 additional fragment ions for proximal and distal chains and over 75 additional fragment ions for *α-endo* and *β-endo* chains per tetramer. Despite exhibiting the same mass shift (addition of 3Ub) at the C-terminus and sharing the same fragment ions regardless of the tetramer analyzed, the identification of fragment ions increased for the distal chains of K48- and K63-linked tetramers (Figure S15b,c) compared to the K6- and K11-linked tetramer (Figure S14a,b). For UVPD + PTCR, the number of matched fragments increased from 12 to 95 (0 to 16 for UVPD alone) as the position of the modified lysine

https://doi.org/10.1021/acs.analchem.3c02618
Anal. Chem. 2023, 95, 14001−14008

shifted from K6 to K63, aside from a slight decrease noted from K29 to K33 (distal chain). The increase in the frequency of identification of C-terminal ions is due to the secondary contribution of C-terminal ions from the other chains of the tetramer. For example, a series of $z14$ to $z75$ ions from all four chains of the K63-linked tetramer contribute to the 95 identified fragment ions (Figure S15c). The increase in the frequency of identification of PTM-containing C-terminal ions (i.e., the density of PTM-containing C-terminal fragment ions) from the distal chain (Figure S15) could be used as evidence to distinguish K48- and K63-linked tetramers.

For both UVPD and UVPD + PTCR, a higher number of fragment ions are identified from the *α-endo* and *β-endo* chains, a feature also reflected in Figure 2 and can be explained by their size. As noted earlier, both N- and C-terminal PTM-containing fragment ions from the *α-* and *β-endo* chains range from 9.2 to 25 kDa, whereas the PTM-containing fragment ions from the distal and proximal chains are >25 kDa (Table S2). Among the six tetramers analyzed, fewer fragment ions are identified for the *endo* chains of K29- and K33- linked tetramers, as the fragment ions are larger than other tetramers (Table S2). UVPD + PTCR revealed additional C-terminal fragment ions from the proximal chain that localize the modification (a mass shift of 3Ub) to K33 or K48 or K63. For example, the detection of PTM-containing x_{14} to x_{28} ions from the proximal chain of the K63-linked tetramer allows differentiation of the K63-linked tetramer from the K48-linked tetramer. The detection of PTM-containing x_{29} to x_{43} (except x_{36}) ions from the proximal chain of the K48-linked tetramer allows the distinction of the K48-linked tetramer from the K33-linked tetramer. However, fewer unique C-terminal fragment ions are identified from the proximal chains because those fragment ions are larger for the K33-, K29-, K11-, and K6-linked tetramers. For example, only two fragment ions (y_{44} and x_{49}, both >30.6 kDa) are identified that afford differentiation of the K33 vs K29 tetramers; only three fragment ions (y_{45}, y_{61}, and y_{62}, 31.8−32.6 kDa) are identified that allow distinction of the K29 vs K11 tetramers.

Collectively, monitoring the $a/a + 1$ ions from the *β/α-endo* chains and the *x*-ions from the proximal chain and mapping the frequency and number of C-terminal ions from the distal chain allow the differentiation of the six tetramers. UVPD promoted extensive fragmentation, and the use of PTCR decongested the resulting MS/MS spectra, allowing far more fragment ions to be assigned that confirmed linkage sites of the K6-, K11-, K29-, K33-, K48-, and K63-linked tetramers. We compared the sequence maps from UVPD + PTCR experiments to those obtained using ETciD in a prior study[34] (Figure S16a−d) for Lys48- and Lys63-linked tetraubiquitin. In Figure S16a−d, more fragment ions that bracket the modifications are observed upon UVPD + PTCR than compared to ETciD for each of the four chains for Lys48- and Lys63-linked tetramers. Additionally, UVPD + PTCR outperforms EThcD for the K29-linked tetramer (Figure S16e,f). This additional level of confidence in characterization holds the potential for analyzing of branched chains and should complement previously established ETciD-based methods to distinguish the topology and linkage sites.[34]

CONCLUSIONS

We capitalized on the attributes of UVPD to generate informative PTM-localizing fragment ions and PTCR to decongest the MS/MS spectra and harvest additional structurally specific fragment ions. We used the PTM-containing ions to map the linkage sites for six unbranched ubiquitin tetramers linked at Lys6, Lys11, Lys29, Lys33, Lys48, and Lys63, respectively. PTCR increased the identification of PTM-containing fragment ions larger than the size of a Ub monomer (8.6 kDa), including ones up to the size of a Ub tetramer (34 kDa). Both UVPD and UVPD + PTCR unambiguously allowed the assignment of the six isomeric tetramers based on the PTM-containing $a/a + 1$ ions from *β-endo* chains. Additionally, the information obtained from the *α-endo* chains allowed the distinction of K6- and K11-linked tetramers, K48- and K63-linked tetramers, and K29-/K33-tetramers from others. Although confident differentiation of the K29- and K33-linked tetramers was not attained from the $a/a + 1$ ions, the gain in PTM-containing C-terminal ions from the *α-endo* chains upon PTCR afforded confident differentiation of K33- and K29-linked tetramers based on the increased frequency of C-terminal ions for K33-linked tetramers. Likewise, the number/frequency of PTM-containing C-terminal ions for the proximal/distal chains of the K63-linked tetramer was much higher than that for the K48-linked tetramers. By using the fragmentation maps produced by UVPD + PTCR to dissect the four Ub chains of each tetramer systematically and imprinting the backbone cleavage sites from which the PTM-containing fragment ions originated on different templates modeling each linkage configuration, we successfully elucidated the linkage sites of each Ub moiety (*β-endo*, *α-endo*, proximal, or distal) within the tetramers were successfully elucidated.

ASSOCIATED CONTENT

Supporting Information

The Supporting Information is available free of charge at https://pubs.acs.org/doi/10.1021/acs.analchem.3c02618.

Detailed experimental section, sequences and linkage patterns of six Ub tetramers, theoretical N-terminal and C-terminal fragment ions and monoisotopic masses, MS1, UVPD, and UVPD + PTCR mass spectra, PTCR window optimization, isotopic distributions of several fragment ions identified by UVPD + PTCR, numbers and distributions of PTM-containing fragment ions for four chains of the six Ub tetramers, backbone cleavage maps of PTM-containing fragment ions, and complete sequence maps (PDF)

AUTHOR INFORMATION

Corresponding Author

Jennifer S. Brodbelt − *Department of Chemistry, University of Texas at Austin, Austin, Texas 78712, United States;* orcid.org/0000-0003-3207-0217; Email: jbrodbelt@cm.utexas.edu

Authors

Aarti Bashyal − *Department of Chemistry, University of Texas at Austin, Austin, Texas 78712, United States;* orcid.org/0000-0003-3559-4534

Sean D. Dunham − *Department of Chemistry, University of Texas at Austin, Austin, Texas 78712, United States;* orcid.org/0000-0002-6214-7468

Complete contact information is available at: https://pubs.acs.org/10.1021/acs.analchem.3c02618

Notes

The authors declare no competing financial interest.

■ ACKNOWLEDGMENTS

Funding from NSF (CHE2203602), the Robert A. Welch Foundation (F-1155), and the UT System for support of the UT System Proteomics Core Facility Network is gratefully acknowledged. We appreciate helpful discussions with Michael Lanzillotti.

■ REFERENCES

(1) Komander, D.; Rape, M. *Annu. Rev. Biochem.* **2012**, *81* (1), 203−229.
(2) Qin, B.; Zhou, L.; Wang, F.; Wang, Y. *Biochem. Pharmacol.* **2022**, *206*, No. 115352.
(3) Xu, P.; Duong, D. M.; Seyfried, N. T.; Cheng, D.; Xie, Y.; Robert, J.; Rush, J.; Hochstrasser, M.; Finley, D.; Peng, J. *Cell* **2009**, *137* (1), 133−145.
(4) Wagner, S. A.; Beli, P.; Weinert, B. T.; Nielsen, M. L.; Cox, J.; Mann, M.; Choudhary, C. *Mol. Cell. Proteomics* **2011**, *10* (10), No. M111.013284.
(5) Mendes, M. L.; Fougeras, M. R.; Dittmar, G. *J. Proteomics* **2020**, *215*, No. 103634.
(6) Park, C.-W.; Ryu, K.-Y. *BMB Rep.* **2014**, *47* (9), 475−482.
(7) Heap, R. E.; Gant, M. S.; Lamoliatte, F.; Peltier, J.; Trost, M. *Biochem. Soc. Trans.* **2017**, *45* (5), 1137−1148.
(8) Popovic, D.; Vucic, D.; Dikic, I. *Nat. Med.* **2014**, *20* (11), 1242−1253.
(9) Walden, H.; Muqit, M. M. K. *Biochem. J.* **2017**, *474* (9), 1439−1451.
(10) Ciechanover, A.; Schwartz, A. L. *Biochim. Biophys. Acta, , Mol. Cell Res.* **2004**, *1695* (1), 3−17.
(11) Deol, K. K.; Strieter, E. R. *Curr. Opin. Chem. Biol.* **2021**, *63*, 95−104.
(12) Huang, Q.; Zhang, X. *Proteomics* **2020**, *20* (9), No. 1900100.
(13) French, M. E.; Koehler, C. F.; Hunter, T. *Cell Discov* **2021**, *7* (1), 1−10.
(14) Dang, F.; Nie, L.; Wei, W. *Cell Death Differ.* **2021**, *28* (2), 427−438.
(15) Heap, R. E.; Gant, M. S.; Lamoliatte, F.; Peltier, J.; Trost, M. *Biochem. Soc. Trans.* **2017**, *45* (5), 1137−1148.
(16) Xu, P.; Duong, D. M.; Seyfried, N. T.; Cheng, D.; Xie, Y.; Robert, J.; Rush, J.; Hochstrasser, M.; Finley, D.; Peng, J. *Cell* **2009**, *137* (1), 133−145.
(17) Kaiser, P.; Wohlschlegel, J. Identification of Ubiquitination Sites and Determination of Ubiquitin-Chain Architectures by Mass Spectrometry. In *Methods in Enzymology; Ubiquitin and Protein Degradation; Part B*; Academic Press, 2005; vol *399*; pp 266−277.
(18) Kim, W.; Bennett, E. J.; Huttlin, E. L.; Guo, A.; Li, J.; Possemato, A.; Sowa, M. E.; Rad, R.; Rush, J.; Comb, M. J.; Harper, J. W.; Gygi, S. P. *Mol. Cell* **2011**, *44* (2), 325−340.
(19) Peng, J.; Schwartz, D.; Elias, J. E.; Thoreen, C. C.; Cheng, D.; Marsischky, G.; Roelofs, J.; Finley, D.; Gygi, S. P. *Nat. Biotechnol.* **2003**, *21* (8), 921−926.
(20) Witze, E. S.; Old, W. M.; Resing, K. A.; Ahn, N. G. *Nat. Methods* **2007**, *4* (10), 798−806.
(21) Crowe, S. O.; Rana, A. S. J. B.; Deol, K. K.; Ge, Y.; Strieter, E. R. *Anal. Chem.* **2017**, *89* (8), 4428−4434.
(22) Rana, A. S. J. B.; Ge, Y.; Strieter, E. R. *J. Proteome Res.* **2017**, *16* (9), 3363−3369.
(23) Xu, P.; Peng, J. *Anal. Chem.* **2008**, *80* (9), 3438−3444.
(24) Valkevich, E. M.; Sanchez, N. A.; Ge, Y.; Strieter, E. R. *Biochemistry* **2014**, *53* (30), 4979−4989.
(25) Swatek, K. N.; Usher, J. L.; Kueck, A. F.; Gladkova, C.; Mevissen, T. E. T.; Pruneda, J. N.; Skern, T.; Komander, D. *Nature* **2019**, *572*, 533−537.
(26) Sun, M.; Zhang, X. *Cell Biosci.* **2022**, *12* (1), 126.
(27) Hospenthal, M. K.; Mevissen, T. E. T.; Komander, D. *Nat. Protoc.* **2015**, *10* (2), 349−361.
(28) Lee, A. E.; Geis-Asteggiante, L.; Dixon, E. K.; Kim, Y.; Kashyap, T. R.; Wang, Y.; Fushman, D.; Fenselau, C. *J. Mass Spectrom.* **2016**, *51* (4), 315−321.
(29) Chen, D.; Gomes, F.; Abeykoon, D.; Lemma, B.; Wang, Y.; Fushman, D.; Fenselau, C. *Anal. Chem.* **2018**, *90* (6), 4032−4038.
(30) Cannon, J. R.; Martinez-Fonts, K.; Robotham, S. A.; Matouschek, A.; Brodbelt, J. S. *Anal. Chem.* **2015**, *87* (3), 1812−1820.
(31) Brodbelt, J. S.; Morrison, L. J.; Santos, I. *Chem. Rev.* **2020**, *120* (7), 3328−3380.
(32) Greer, S. M.; Brodbelt, J. S. *J. Proteome Res.* **2018**, *17* (3), 1138−1145.
(33) Walker, J. N.; Lam, R.; Brodbelt, J. S. *Anal. Chem.* **2023**, *95* (14), 5985−5993.
(34) Lee, A. E.; Geis-Asteggiante, L.; Dixon, E. K.; Miller, M.; Wang, Y.; Fushman, D.; Fenselau, C. *J. Mass Spectrom.* **2016**, *51* (8), 629−637.
(35) Cammarata, M. B.; Thyer, R.; Rosenberg, J.; Ellington, A.; Brodbelt, J. S. *J. Am. Chem. Soc.* **2015**, *137* (28), 9128−9135.
(36) Shaw, J. B.; Li, W.; Holden, D. D.; Zhang, Y.; Griep-Raming, J.; Fellers, R. T.; Early, B. P.; Thomas, P. M.; Kelleher, N. L.; Brodbelt, J. S. *J. Am. Chem. Soc.* **2013**, *135* (34), 12646−12651.
(37) Sanders, J. D.; Mullen, C.; Watts, E.; Holden, D. D.; Syka, J. E. P.; Schwartz, J. C.; Brodbelt, J. S. *Anal. Chem.* **2020**, *92* (1), 1041−1049.
(38) Holden, D. D.; Brodbelt, J. S. *Anal. Chem.* **2017**, *89* (1), 837−846.
(39) Holden, D. D.; Sanders, J. D.; Weisbrod, C. R.; Mullen, C.; Schwartz, J. C.; Brodbelt, J. S. *Anal. Chem.* **2018**, *90* (14), 8583−8591.
(40) Toby, T. K.; Fornelli, L.; Kelleher, N. L. *Annu. Rev. Anal. Chem.* **2016**, *9* (1), 499−519.
(41) Brown, K. A.; Melby, J. A.; Roberts, D. S.; Ge, Y. *Expert Rev. Proteomics* **2020**, *17* (10), 719−733.
(42) Klein, D. R.; Holden, D. D.; Brodbelt, J. S. *Anal. Chem.* **2016**, *88* (1), 1044−1051.

https://doi.org/10.1021/acs.analchem.3c02618
Anal. Chem. 2023, 95, 14001−14008